NASA Technical Memorandum 82732

Effects of Artificially Produced Defects on Film Thickness Distribution in Sliding EHD Point Contacts

C. Cusano
University of Illinois at Urbana-Champaign
Urbana, Illinois

and

L. D. Wedeven
Lewis Research Center
Cleveland, Ohio

Prepared for the
Joint Lubrication Conference
cosponsored by the American Society of Lubrication Engineers
and the American Society of Mechanical Engineers
New Orleans, Louisiana, October 5-7, 1981

NASA

EFFECTS OF ARTIFICIALLY PRODUCED DEFECTS ON FILM THICKNESS DISTRIBUTION IN SLIDING EHD POINT CONTACTS

C. Cusano
Department of Mechanical and Industrial Engineering
University of Illinois at Urbana-Champaign
Urbana, Illinois 61801

L. D. Wedeven
National Aeronautics and Space Administration
Lewis Research Center
Cleveland, Ohio 44135

ABSTRACT

The effects of artificially produced dents and grooves on the elastohydrodynamic (EHD) film thickness profile in a sliding point contact are investigated by means of optical interferometry. The defects, formed on the surface of a highly polished ball, are held stationary at various locations within and in the vicinity of the contact region while the disk is rotating. It is shown that the defects, having a geometry similar to what can be expected in practice, can dramatically change the film thickness which exists when no defects are present in or near the contact. This change in film thickness is mainly a function of the position of the defects in the inlet region, the geometry of the defects, the orientation of the defects in the case of grooves, and the depth of the defect relative to the central film thickness.

E-1042

INTRODUCTION

The tribological behavior of contacting surfaces can be influenced by the topography of the surfaces. The degree of influence mainly depends on minimum film thickness and the topographical features of the surfaces. Such influence is especially acute in elastohydrodynamic (EHD) contacts where the minimum film thickness and the surface irregularities can be of the same order of magnitude. Under these conditions, both analytical and experimental studies of the contact are very difficult. Because of this difficulty, there has been a tendency to simplify real rough surfaces with surfaces which can be more easily analyzed. These simplifications have been made by considering only transverse or longitudinal roughness, by artifically producing "rough" surfaces and defects, and by analyzing single asperities or furrows.

Transverse and longitudinal roughness and idealized asperities in EHD contacts have been analytically studied by Chow and Cheng [1,2].* Experimental investigations of a debris dent, and artifically produced dents, furrows and rough surfaces in EHD contacts have been conducted by Wedeven [3], Wedeven and Cusano [4], Cusano and Wedeven [5], Jackson and Cameron [6], and Kaneta and Cameron [7]. By means of optical interferometry, references [3-6] have demon-

*Numbers in brackets designate References at end of paper.

strated that large film thickness variations can occur around surface defects. These film thickness variations can cause a reduction in film thickness resulting in possible scuffing failures and/or an increase in local film thickness with accompanying high localized pressure and stresses resulting in possible fatigue failures. An important first step in determining these pressures and stresses around furrows and asperities in line contact has been made by the analytical work of Cheng and Bali [8].

The above studies have demonstrated a number of geometrical and topographical features which are important when considering dents, furrows, and rough surfaces in EHD contacts. These features and the kinematics of the contacting surfaces influence the film thickness distribution and, therefore, the pressure distributions in such contacts. Specifically, it has been found that this film thickness distribution is mainly influenced by the following:

1. Surface lay, i.e., whether the surface roughness is longitudinal or transverse relative to the direction of flow.

2. Whether surfaces are under pure rolling or pure sliding conditions.

3. Size of surface irregularities in comparison to the central film thickness based on smooth surfaces.

4. Slopes of irregularities.

5. Position of irregularities within the Hertzian region.

6. In contacts between rough and smooth surfaces, whether the rough surfaces is moving or stationary under simple sliding conditions.

In [4,5], the film thickness variations caused by **artificially-produced** irregularities on highly polished balls in contact with a sapphire disk were observed under pure rolling and pure sliding conditions. The surface irregularities were observed by taking high-speed single-flash photography. A xenon flash lamp was synchronized with the ball rotation and could be delayed so that the irregularities could be photographed in various positions within the conjunction region. In order to obtain data under pure sliding conditions, the disk was momentarily stopped manually while the ball rotated. Under these conditions, it was not an easy task to position the irregularities or defects arbitrarily within the inlet region of contact.

The primary emphasis of the present work is also the determination, by optical interferometry, of the film thickness variations caused by artificially-produced dents and furrows in simple EHD sliding contacts. As in [4,5], the defects are formed on a highly polished ball which is in contact with a sapphire disk. However, in the present work, the ball and, therefore, the defects are held stationary at various positions in the inlet region and Hertzian contact while the disk is moving. Unlike the previous work, in the present work, the defects could be easily positioned anywhere and therefore, a more complete investigation of the effects of surface defects on film thickness variations was possible.

EXPERIMENTAL APPARATUS

As stated previously, the film thickness distribution within the Hertzian contact was observed by using optical interferometry. The optical elastohydrodynamic apparatus is shown in Fig. 1 and described in detail elsewhere [9,10]. The basic components of the apparatus consist of a ball which rides against a transparent disk.

Fringes of very good visibility were obtained by using a 17 percent reflecting layer of chromium on the bearing surface of the transparent disk. Interference measurements were made with wavelengths of two colors (red and green). These were obtained by using a special filter and a xenon flash lamp as a light source. The details of this system and its calibration are described more fully in [11,12]. All measurements were carried out at room temperature.

TEST MATERIALS

The test bearing specimens are shown in Fig. 2. The ball is 0.02063 m in diameter and made of AISI 52100 steel. Its nominal surface roughness is better than 0.018 μm rms (0.7 μin.) and its hardness is approximately 65 R_c. Other mechanical properties are shown in Table 1. The transparent disk is 0.102 m in diameter and made of sapphire. Its mechanical properties are also given in Table 1.

The test ball was supported by three bearings located in a lubricant reservoir shown in Fig. 2. The formation of the artificial defects on the ball is described in detail in [4].

The tests were performed with a synthetic paraffinic oil that was designated by the manufacturer as XRM 109F3. The properties of the test fluid are given in Table 2.

RESULTS

The surface defects were observed at various positions in the conjunction region by taking single-flash photographs. Stylus traces through the deepest part of the "undeformed" defects were also taken after the testing program on each defect had been completed. The data to be presented will show stylus traces of the defects followed by photographs of the same defects progressively positioned closer to the inlet and in the contact region. Unlike the detailed film thickness distribution plots presented in previous papers [3-5], the present work will emphasize more general aspects of oil film distributions and their variations from the smooth-surface values caused by the defects. For all the figures which will be presented, the inlet is at the right-hand side of the figure and exit is at the left-hand side. A given defect is shown in the same orientation in the stylus traces and in the conjunction regions.

Three parameters are used to specify the geometry and position of most of the defects. The position is specified by $X = X/a$ where X is the distance from the center of the Hertzian contact to the center (deepest part) of single dents or single transverse grooves, or to the center (deepest part) of the groove closest to the contact for multiple transverse grooves, or to the tip of longitudinal grooves and "a" is the contact radius. The width of the defects is specified by $C = c/a$ where c is one-half of the largest width

of single defects or one-half of the largest width of the groove closest to the contact for multiple transverse grooves. The depth of the defects is specified by the parameter $\Delta = \delta/h_0$, where δ is the maxium depth of single defects or the maximum depth of the groove closest to the contact for multiple transverse grooves and h_0 is the central film thickness based on smooth surfaces. Because most of the defects have built-up edges, the value of c and δ are obtained by extending the smooth-surface profile, on both sides of the defects, as shown in Fig. 5. Also note from Fig. 5 that in approximating the value of c, the rounded edges (left-hand side of dent) are not considered.

The stylus trace through the deepest portion of a dent is shown in Fig. 3. This dent is the same as the dent shown in Figs. 3 and 4 of [4]. For this dent, $\Delta = 6.3$ and $C = 0.32$. Figures 4(a) to (d) show the dent at various positions in the inlet and Hertzian contact. In Fig. 4(a) the dent is far enough from the inlet that it does not influence the film thickness in the contact. In Fig. 4(b) the dent influences the inlet pressure generation, and therefore, the pressure in the contact, resulting in an overall reduction of film thickness from 0.16 μm (Fig. 4(a)) to 0.10 μm. This reduction takes place in a band, downstream (left of dent) in the direction of motion, approximately equal to the width of the dent. In Fig. 4(c) micro-EHD effects increase the film thickness in this band to a value above the smooth-surface value of 0.16 μm, and in Fig. 4(d) the film thickness in the band is still above the smooth-surface value but below the maximum value obtained in Fig. 4(c). In Fig. 4(d) it is noted that complete film recovery, to the smooth-surface value, occurs upstream (to the right) of the dent. The same dent under pure sliding conditions and approximately the same smooth-surface film thickness, but with the ball moving and the disk stationary, is shown in Figs. 7(a) to (c) of [4]. Comparing the film thickness variations in these figures to those in the present work, it can be concluded that with a moving dent and stationary disk the film thickness variations are more localized than when the dent is stationary and the disk is moving. Excluding the area in the immediate vicinity of the dent, the film thickness variations occur on the exit side of the dent when the dent is stationary and on the inlet side when the dent is moving. Such differences can be explained by considering the kinematics of the contacting surfaces and the geometry of the dent.

In Figs. 5 and 6(a) to (d) a dent with a $\Delta = 3.8$ and $C = 0.42$ is shown. In Fig. 6(a) the position of the dent does not influence the central film thickness which, in this case, is 0.26 μm. The general trends shown in Fig. 6 are the same as those shown in Fig. 4. An even larger dent is shown in Figs. 7 and 8(a) to (g) for which $\Delta = 6.7$ and $C = 0.53$. Note that the film thickness variations again occur within a band which is approximately equal to the width of the dent. From Fig. 8(g) it is noted that, once the dent is within the contact, the film thickness variations are more localized in the vicinity of the dent and that complete film recovery again occurs upstream of the dent. In Fig. 9, a cross-sectional plot of the dent corresponding to its position in Fig. 8(g) is shown to indicate the micro-EHD effects caused by the built-up edge on the right-hand side of the dent (see Fig. 7). A stylus trace of the dent is also shown in Fig. 9. The position of this trace is such that its horizontal line corresponds to the smooth-surface central film thickness of 0.26 μm. As with previous finding [5], it is noted that the stylus trace of the "undeformed" dent predicts contact between the surfaces while the trace

from Fig. 8(g) shows the existence of a film and considerable deformations in the vicinity of the built-up edge. In addition, note that, with this larger dent, the downstream film thickness is approximately equal to or below the smooth-surface value once the dent enters the contact.

Even though the three dents discussed above have different geometries, some general trends can be observed. The dents shown in Figs. 3 and 7 have values of Δ which are approximately the same while the values of C are quite different. Figure 4 shows that the maximum percentage change in the central film thickness, from its smooth surface value, varies from -37 to 44 percent while from Fig. 8, this change is from -38 to 46 percent. Thus, it is noted that, for approximately the same Δ, approximately the same percentage changes in film thickness are observed. For the dent shown in Fig. 5, the value of Δ is much smaller than the Δ values of the dents shown in Figs. 3 and 7. From Fig. 6, the maximum percentage change in film thickness from the smooth-surface value varies from -27 to 54 percent. These findings suggest that Δ is a useful parameter for predicting the changes in the central film thickness, from its smooth-surface value, caused by dents.

The effects of X, the position parameter, on the film thickness distribution is shown in Fig. 10 where the data given in Figs. 6 and 8 are shown in a more compact form. In this figure $H = h/h_0$ where h is the film thickness downstream of the dent and h_0 is the central film thickness based on smooth surfaces. Since the film thickness is only known at discrete values of X, the lines connecting the data points do not represent actual film thickness distribution but only general trends. Although not shown in Fig. 10, the data given in Fig. 4 follow the same pattern.

In Figs. 11 and 12(a) to (d), a relatively shallow groove is shown with a $\Delta = 1.4$ and $C = 0.11$. As with the dents, it is seen from Fig. 12(b) that the smooth-surface film thickness is reduced when the groove approaches the inlet. As the groove enters the contact, a comparison between Figs. 12(a) and (d) shows that the film completely recovers except in localized areas around the groove.

A deeper groove is shown in Figs. 13 and 14(a) to (e). For this groove, $\Delta = 3.4$ and $C = 0.08$. Again, the central film thickness is not affected when the groove is located far enough from the inlet as shown in Fig. 14(a). In Figs. 14(b) and (c) a film reduction is seen when the groove is in the inlet region while a partial film recovery downstream of the groove (to its left) takes place as the groove enters the contact as shown in Figs. 14(d) and (e). Note that unlike the previous groove, this recovery is less than the smooth-surface value. As before, upstream of the groove, a full film recovery takes place. Since continuity of flow has to exist, some fluid has to be "drained" along the groove in order to obtain the change in film thickness between the upstream and downstream sections of the groove as shown in Fig. 14(e). Similar effects have been found with a moving deep groove and a stationary disk as indicated by Fig. 22 of [4]. Figure 14(e) also shows considerable micro-EHD effects caused by a built-up edge in this area (see Fig. 13). In Fig. 15 a partial cross-sectional plot of the film thickness at the edges of the groove is shown to indicate the large deformations caused by this micro-EHD action. In this figure the horizonal line of the stylus trace is positioned at the smooth-surface central film thickness as done previously with the dent. Again, note that the stylus trace of the "undeformed" groove predicts contact between the surfaces while the measured profile shows the existence of a film.

A groove having a $\Delta = 2.7$ and $C = 0.12$, located longitudinal to the direction of flow, is shown in Figs. 16 and 17(a) to (c). The behavior of this groove, in the conjunction region, is quite similar to the behavior of similar grooves studied in [4] where the grooves were moving and the disk was stationary. Figure 17 shows that the film thickness variations caused by the groove are localized around the grove itself. The groove does not affect the film thickness throughout the contact as done by grooves oriented in the transverse direction. This behavior can be understood by noting that, for a longitudinal groove, the inlet pressure is only changed over a band approximately equal to the width of the groove.

Three closely spaced grooves are shown in Figs. 18 and 19(a) to (d). The values of Δ and C for the groove closest to the inlet are 2.8 and 0.15, respectively. Again, it is seen that as soon as the grooves enter the inlet region, a reduction in film thickness occurs downstream of the grooves as shown in Fig. 19(b). Figures 19(c) and (d) show that as the grooves pass the inlet region, there is a complete recovery of the film upstream of the grooves and a partial recovery downstream of the grooves. As with the grooves in Fig. 14, some oil drainage along the groove occurs. By comparing the results from Fig. 19 to those shown in Figs. 17(b) and 30 of [5], for approximately the same central film thickness, again it can be concluded that the film thickness variations are more widespread throughout the contact when the grooves are stationary and the disk is moving than when the grooves are moving and the disk is stationary.

Because of the diverse geometries of the groove, direct comparisons between the various film thickness distributions caused by these grooves cannot be made. It can again be stated, however, that Δ plays an important role. The grooves shown in Figs. 11 and 13 have a Δ of 1.4 and 3.4, respectively. The reduction in central film thickness, from the smooth-surface value, is 27 percent for the groove shown in Fig. 11 and 62 percent for the groove shown in Fig. 13.

DISCUSSION

The data presented in this paper indicate that for the same smooth-surface central film thickness, more film thickness variations are caused by stationary defects than by moving defects under pure sliding conditions. One possible explanation for such difference is that the defects are in the conjunction region for a relatively short period of time when they are moving and the disk is stationary. Therefore, thermal effects, converging-wedge effects, as well as fluid drainage effects can be less severe under such kinematic conditions. These findings were also substantiated at the beginning of the testing program when an attempt was made to use the same defects and central film thickness used in [4,5]. By changing the kinematic condition from stationary disk and moving defects used in [4,5] to stationary defects and moving disk used in the present study, it was noted that severe damage was caused to the coating of the disk when the defects were positioned in the inlet region. No coating damage was noted in obtaining the data reported in [4,5]. Because of this coating damage, most of the data presented in this paper were obtained by using a larger central film thickness than that used in references [4,5].

The results presented indicate that defects in or near the contact change the central film thickness obtained with smooth surfaces. This change is

caused by a modification of the local EHD pressure generated in the inlet region of the contact. For a given smooth-surface film thickness, the extent of this change depends on the geometry and location of the defects. With dents, the general pattern, as the dents are progressively positioned closer to the inlet region and finally into the contact, is for the downstream film thickness at first to be lowered from its smooth-surface value, then increase to a maximum which can be much larger than its smooth-surface value and finally decrease to a value which can be larger or smaller, depending on the size of the dent, than the smooth-surface value. The fluid film thickness upstream of the dents is always equal to its smooth-surface value.

For grooves oriented transversely to the direction of flow, the central film thickness is first reduced as the grooves enter the inlet and then it increases as the grooves enter the contact. For shallow grooves, the downstream film thickness increases to its smooth-surface value when the grooves are in the contact while, for deeper grooves, the downstream film thickness never recovers to its smooth-surface value. It is noted that, unlike dents, grooves do not seem to generate downstream central film thicknesses which are larger than the corresponding smooth-surface values. This difference between dents and grooves is probably due to the tendency of the fluid to be trapped within dents while draining along grooves in the inlet region.

The location of the defects, especially in the inlet region, can have a significant influence on the film thickness distribution in the entire contact. The degree of influence is mainly a function of Δ. It can generally be stated that if Δ is small, the variations in film thickness tend to be more localized around the defects while with a large Δ the film thickness can change throughout the contact. In addition, large localized film thickness variations can be caused by built-up edges around defect. Such variations can result in very high stress concentrations in the vicinity of the built-up edges. Since defects can cause these film thickness variations from the smooth surface value, it is reasonable to assume that they can contribute to both fatigue and scuffing failures. Scuffing failures can take place because of the reduction in film thickness from the smooth-surface value and fatigue failures can take place as the result of micro-EHD action which can cause large surface deformations with accompanying high stress concentrations.

It can be argued that the analytical film thickness data obtained for furrows in line contacts should follow the same trends as the experimental data presented in this paper for dents in point contacts. This argument is based on the fact that, for both contacts, the lubricant tends to be trapped within the defects. A complete analytical solution of the line contact problem, recently obtained at the Univeristy of Illinois, substantiate the general film thickness trends reported in this paper for dents. That is, the presence of a furrow close to or within the inlet region in line contacts can decrease or increase the central film thickness, from the smooth-surface value, depending on its position in this region. The analytical line contact data obtained by Cheng and Bali [8], which are based on an analysis of the inlet half of the contact, show a decrease in the film thickness, from the smooth-surface value, for the furrow positions analyzed. It is reasonable to assume that their analysis would also show increases in film thickness, from the smooth-surface value, if more data were obtained with the furrow at various positions within the inlet region and contact.

It is felt that analytical solutions which would consider the same defect geometries and other parameters presented in this paper would indicate that, inside many of the defects, the pressure would go to zero. Perhaps future analytical studies, which consider cavitation in the defects for both line and point contacts, will result in a better understanding of the film thickness variations and associated pressure and stress variations caused by defects.

CONCLUSIONS

The following conclusions can be drawn as the result of this study:

1. The film thickness variations in the Hertzian contact, caused by dents and grooves, are more widespread when the defects are stationary and the disk is moving than when the defects are moving and the disk is stationary.

2. Dents change the central film thickness as they approach and enter the inlet in EHD contacts. The downstream film thickness is first reduced below its smooth-surface value, then increases above its smooth-surface value and finally decreases to a value which is from above to below the smooth-surface value depending on the size of the dent.

3. Grooves oriented transversely to the direction of flow tend to change the central film thickness more dramatically than dents as they approach and enter the inlet. With these grooves, the downstream film thickness is first reduced from its smooth surface value and then, as the grooves progressively move into the contact, the film thickness recovers to its smooth-surface value or stays below this value depending on the size of the grooves.

4. The film thickness upstream of the defects always recovers to the smooth-surface values for all defects considered.

5. The film thickness variations caused by the defects mainly depend on the depth of the defect relative to the central film thickness.

6. Micro-EHD action can produce large local surface deformations with accompanying large stress concentrations near the built-up edges of defects.

REFERENCES

1. Chow, L. S. H. and Cheng, H. S., "Pressure Perturbation in EHD Contacts Due to an Ellipsoidal Asperity," J. Lub. Tech., ASME Trans., 98. Series F, (1), 8-15 (1976).

2. Chow, L. S. H. and Cheng, H. S., "The Effects of Surface Roughness on the Average Film Thickness Between Lubricated Rollers," J. Lub. Tech., ASME Trans., 98, Series F, (1), 117-124 (1976).

3. Wedeven, L. D., "Influence of Debris Dent on EHD Lubrication," ASLE Trans., 21, (1), 41-52 (1978).

4. Wedeven, L. D. and Cusano, C., "Elastohydrodynamic Film Thickness Measurements of Artificially Produced Surface Dents and Grooves," ASLE Trans., 22, (4), 369-381 (1979).

5. Cusano, C. and Wedeven, L. D., "Elastohydrodymanic Film Thickness Measurements of Artificially Produced Nonsmooth Surfaces," ASLE Trans., 24, (1), 1-14 (1981).

6. Jackson, A. and Cameron, A., "An Interferometric Study of the EHL of Rough Surfaces," ASLE Trans., 19, (1), 50-60 (1976).

7. Kaneta, M. and Cameron, A., "Effects of Asperities in Elastohydrodynamic Lubrication," J. Lub. Tech., ASME Trans., 102, Series F, (3), 374-379 (1980).

8. Cheng, H. S. and Bali, M., "Stress Distributions around Furrows and Asperities in EHL Line Contacts," Symposium on Solid Contact and Lubrication. Presented at ASME Winter Annual Meeting, Chicago, Illinois, Nov. 16-21, 1980, Appl. Mech. Div. V. 39, edited by H. S. Cheng and L. M. Kerr, ASME (1980), pp. 205-222.

9. Wedeven, L. D., "Traction and Film Thickness Measurements under Starved Elastohydrodynamic Conditions," J. Lub. Tech., ASME Trans., 97, Series F, (2), 321-329 (1975).

10. Wedeven, L. D., "Effect of Starvation on Film Thickness and Traction under Elastohydrodynamic Rolling and Sliding Conditions," NASA TN D-8087, 1975.

11. Wedeven, L. D., Evans, D., and Cameron, A., "Optical Analysis of Ball Bearing Starvation," J. Lub. Tech., ASME Trans., 93, Series F, (3), 349-363 (1971).

12. Foord, C. A., Wedeven, L. D., Westlake, F. J., and Cameron, A., "Optical Elastohydrodynamics," Proc. Inst. Mech. Engr., 184, pt. 1, (28), 487-505 (1969-1970).

TABLE 1. - BEARING MATERIAL PROPERTIES

	Ball	Disk
Material	52100 Steel	Sapphire
Compressive strength	1.4×10^9 N/m^2	2×10^9 N/m^2
Elastic modulus	204×10^9 N/m^2	365×10^9 N/m^2
Poisson's ratio	0.3	0.25
Hardness	65 R_c	9 Moh
Roughness	0.018 μm rms	Optical polish

TABLE 2. - PROPERTIES OF TEST FLUID

	Synthetic paraffinic oil (XRM 109F3)
Viscosity	45 830 cS at -17.8° C
	493 cS at 37.8° C
	42.6 cS at 98.9° C
Density	0.8389 g/cm^3 at 37.8° C
	0.8082 g/cm^3 at 93.3° C
	0.777 g/cm^3 at 149° C
Pressure viscosity coefficient	1.77×10^{-8} m^2/N at 37.8° C
	1.51×10^{-8} m^2/N at 99° C
	1.09×10^{-8} m^2/N at 149° C
Refractive index	1.4689 at 23° C

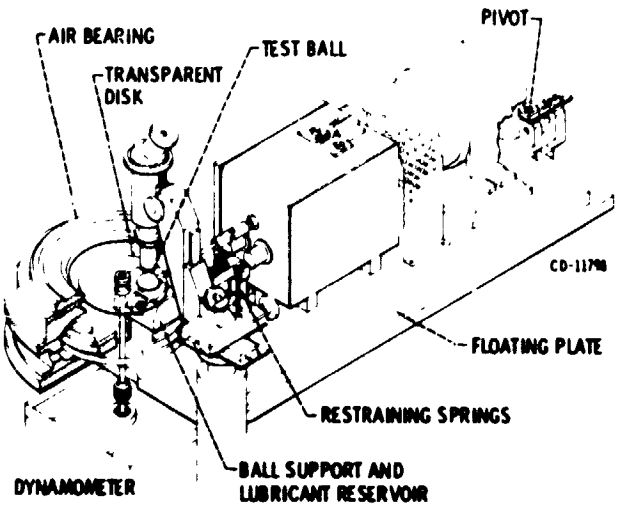

Figure 1. - Optical EHD rig.

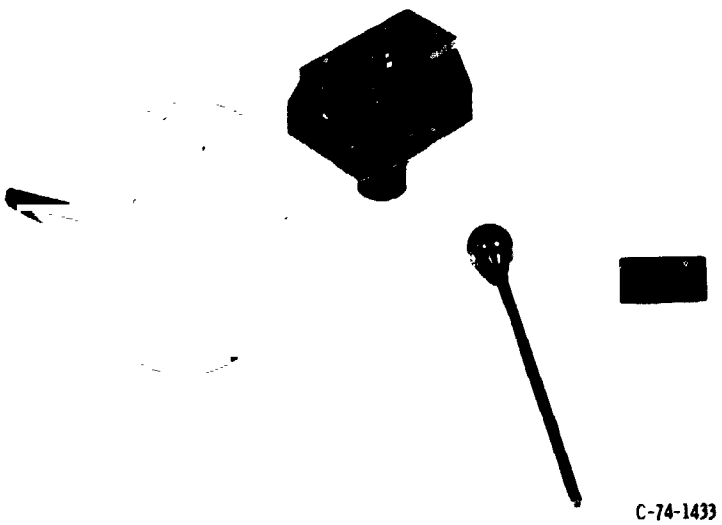

Figure 2. - Test ball, transparent disk and lubricant reservoir.

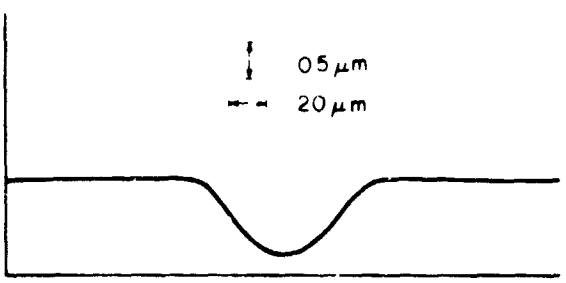

Figure 3. - Stylus trace of small dent, A = 6.3, C = 0.32.

ORIGINAL PAGE
BLACK AND WHITE PHOTOGRAPH

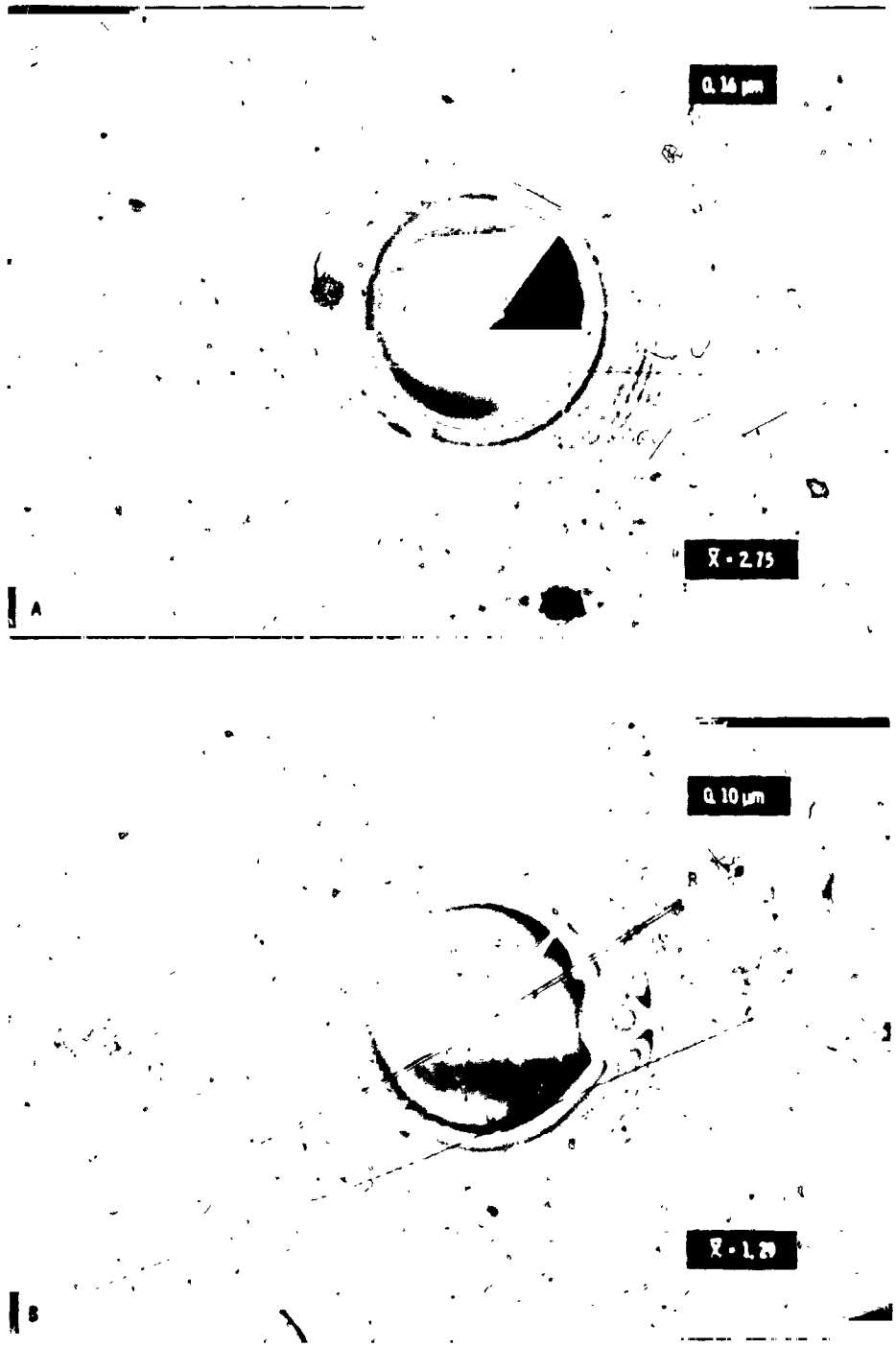

Figure 4. - Small dent progressively positioned closer to inlet and in contact. Disk velocity = 0.06 m/s, P_{max} = 1.13×10^6 N/m^2, T = 23.6° C.

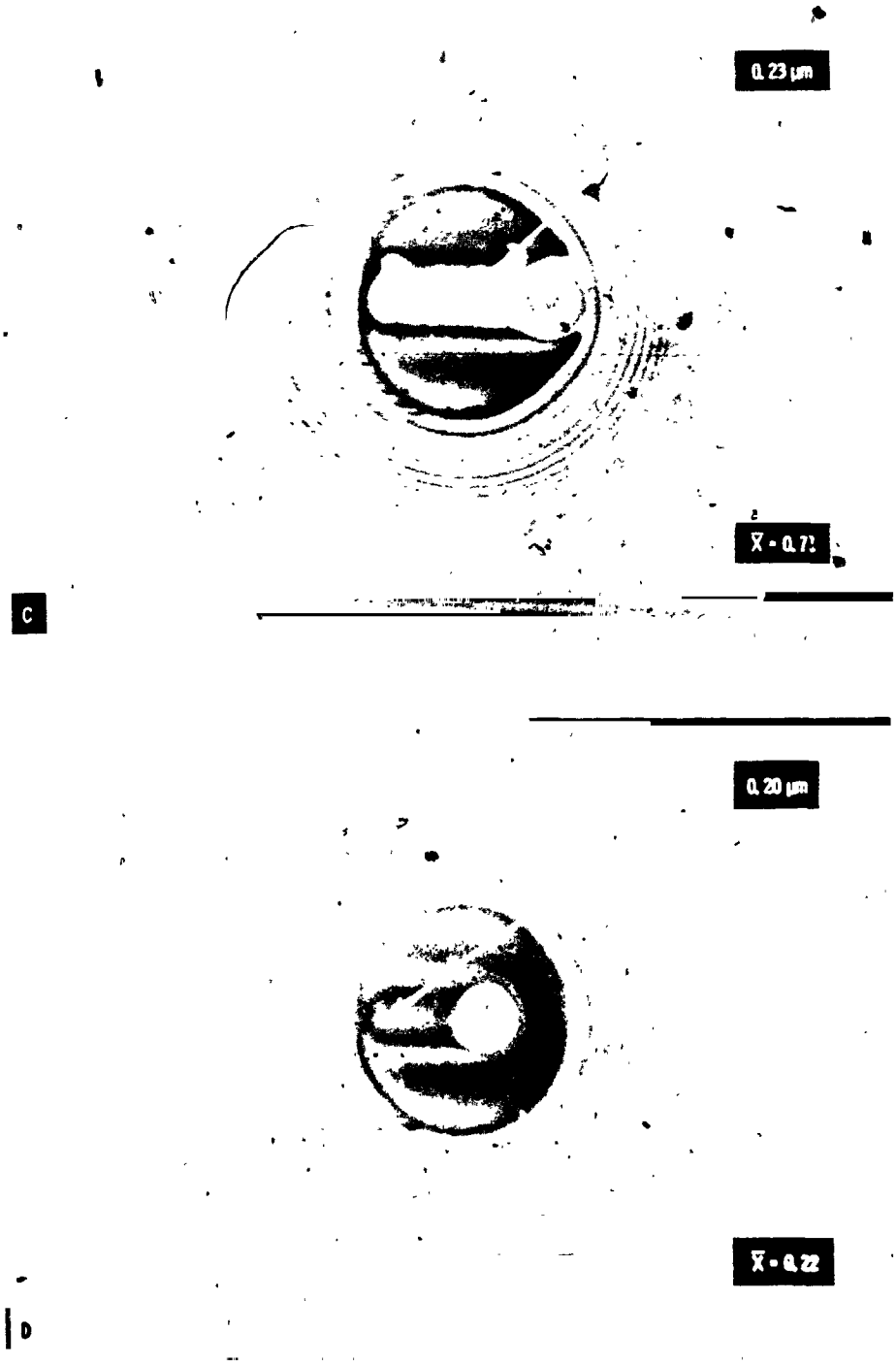

Figure 4. - Concluded.

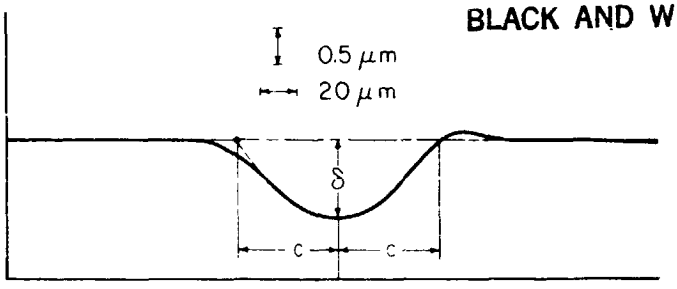

Figure 5. - Stylus trace of medium dent, Δ = 3.8, C = 0.42.

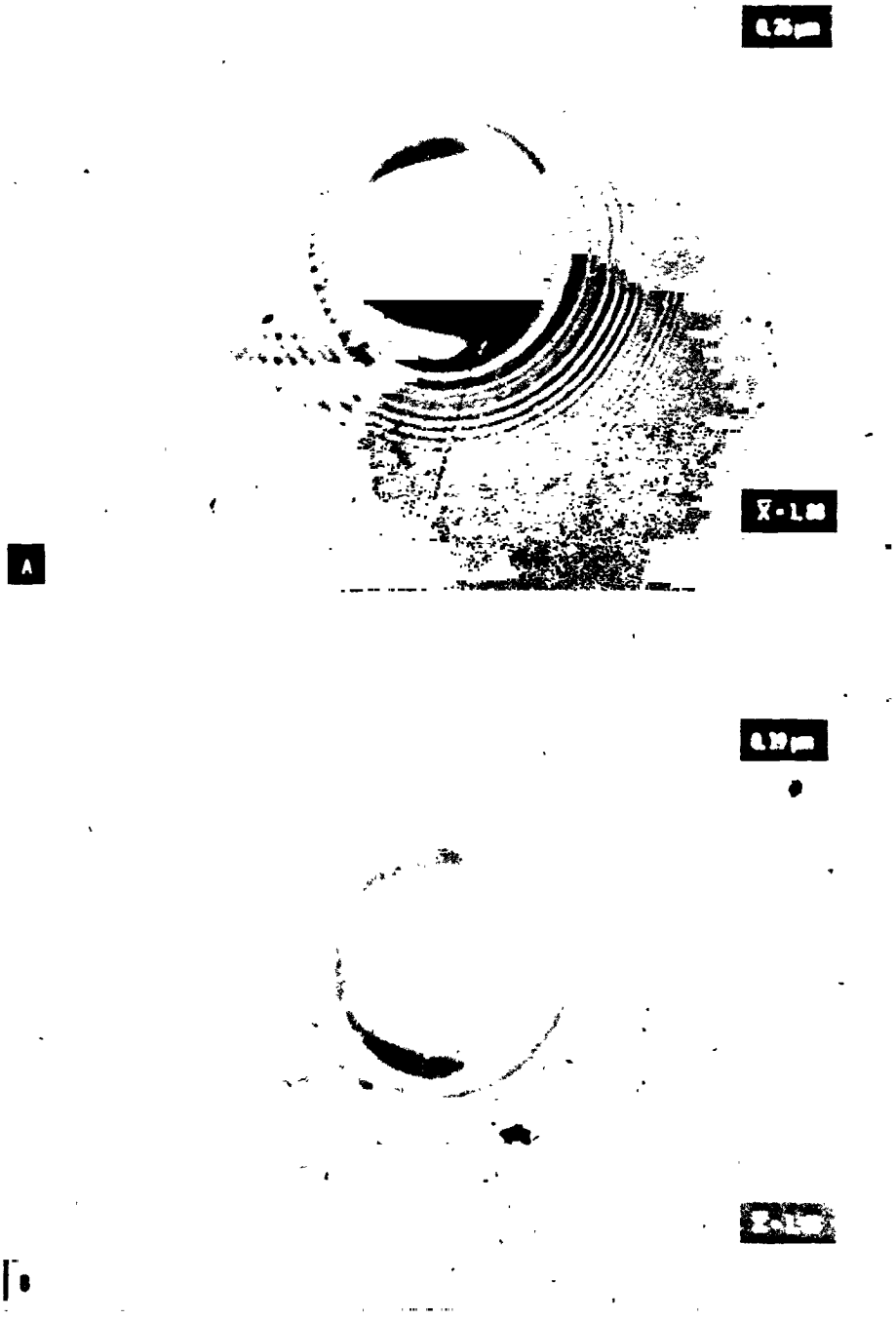

Figure 6. - Medium dent progressively positioned closer to inlet and in contact. Disk velocity = 0.12 m/s, P_{max} = 1.13x10^9/m^2, T = 24.4^0 C.

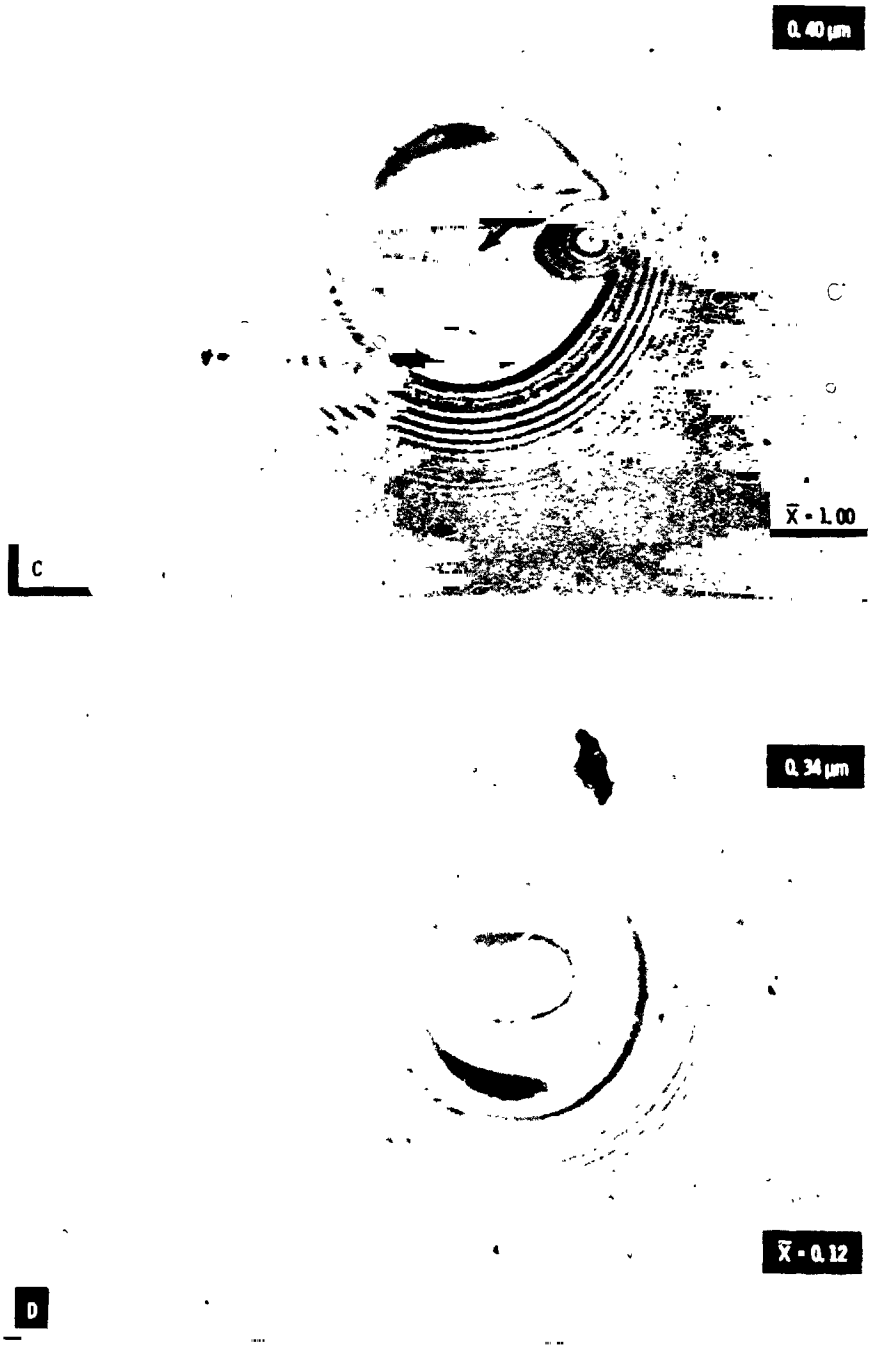

Figure 6. - Concluded.

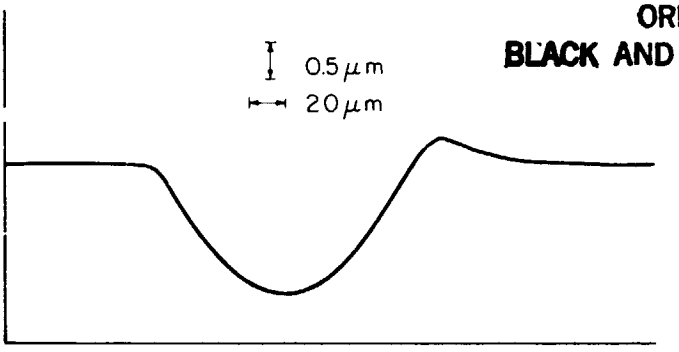

Figure 7. - Stylus trace of large dent, Δ = 6.7, C = 0.53.

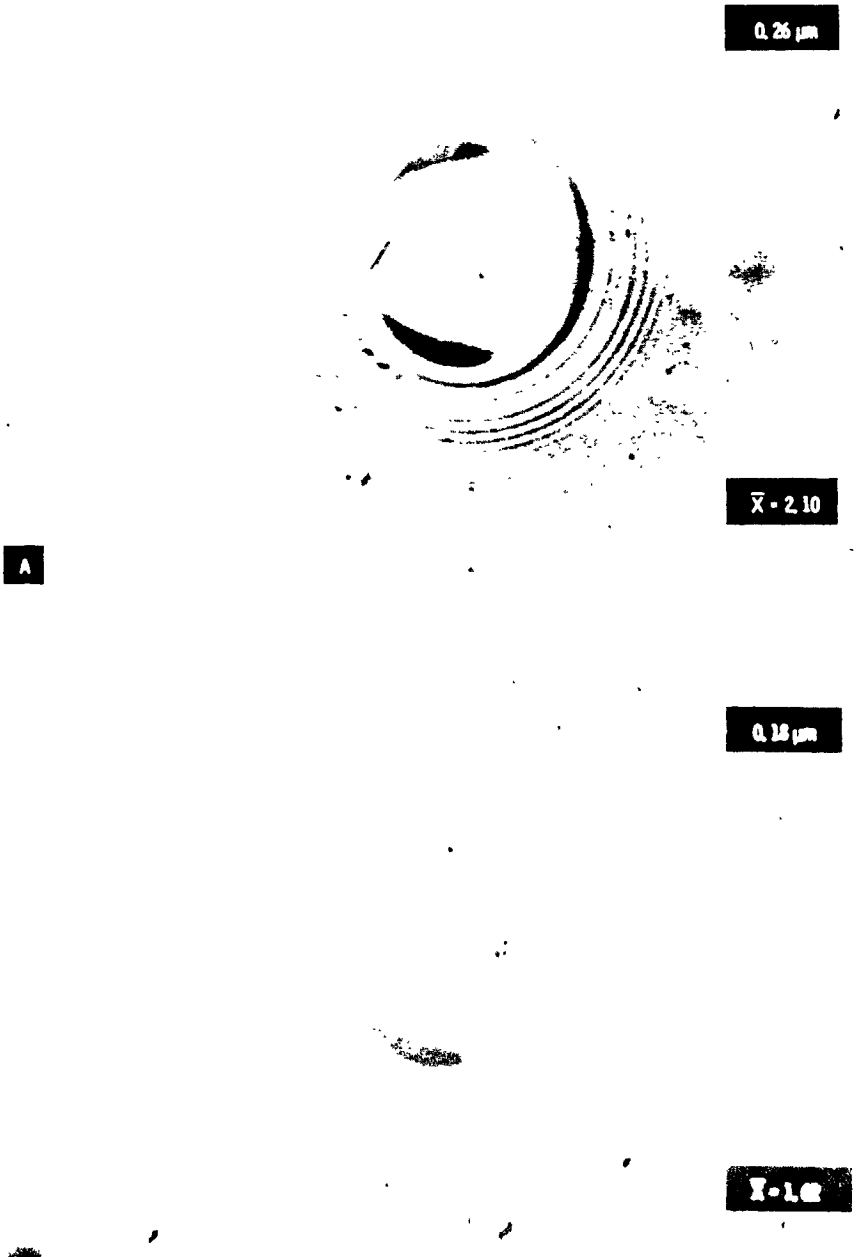

Figure 8. - Large dent progressively positioned closer to inlet and in contact. Disk velocity = 0.12 m/s, P_{max} = 1.13x10^{9} N/m^{2}, T = 24.4° C.

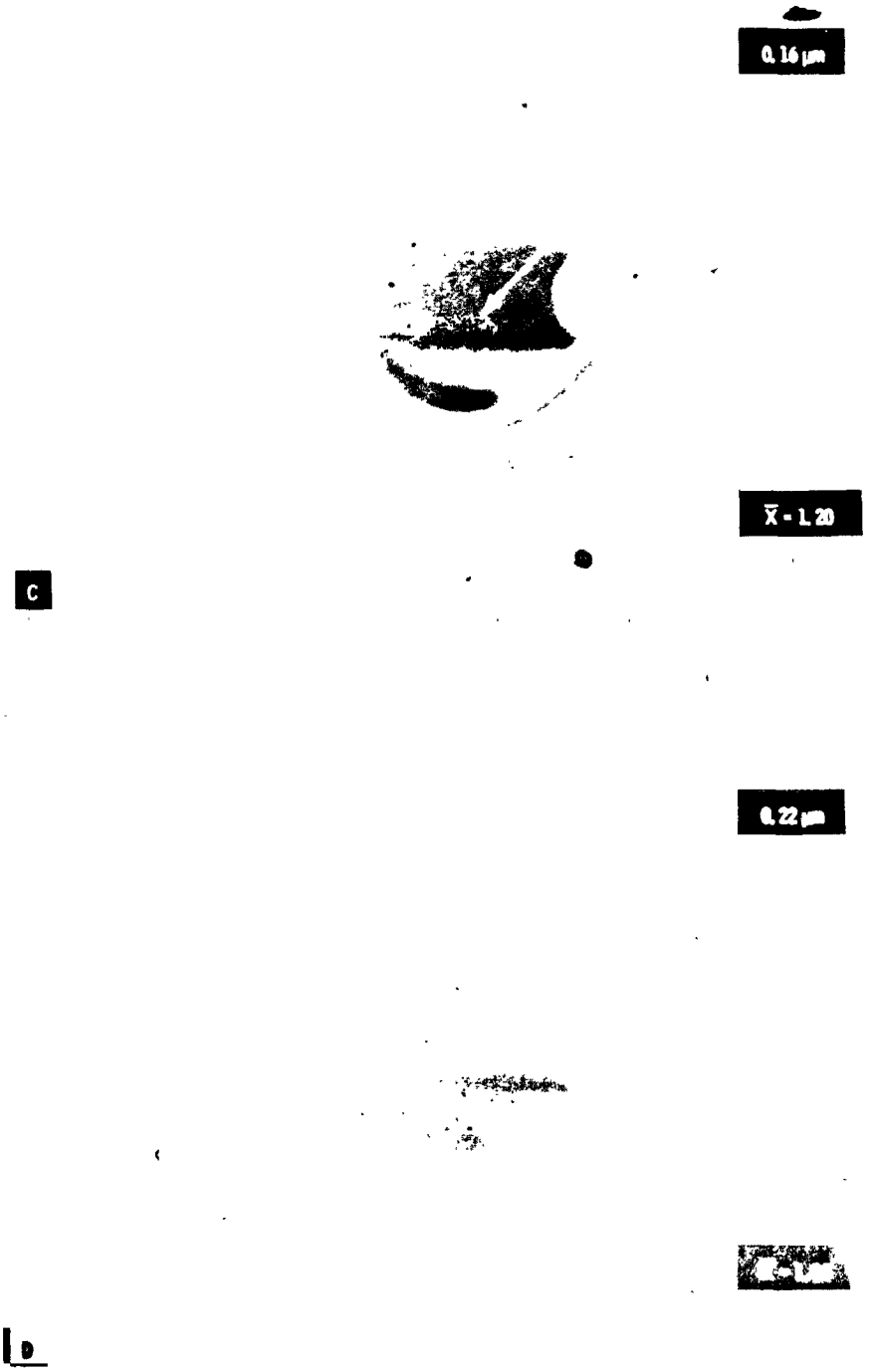

Figure 8. - Continued.

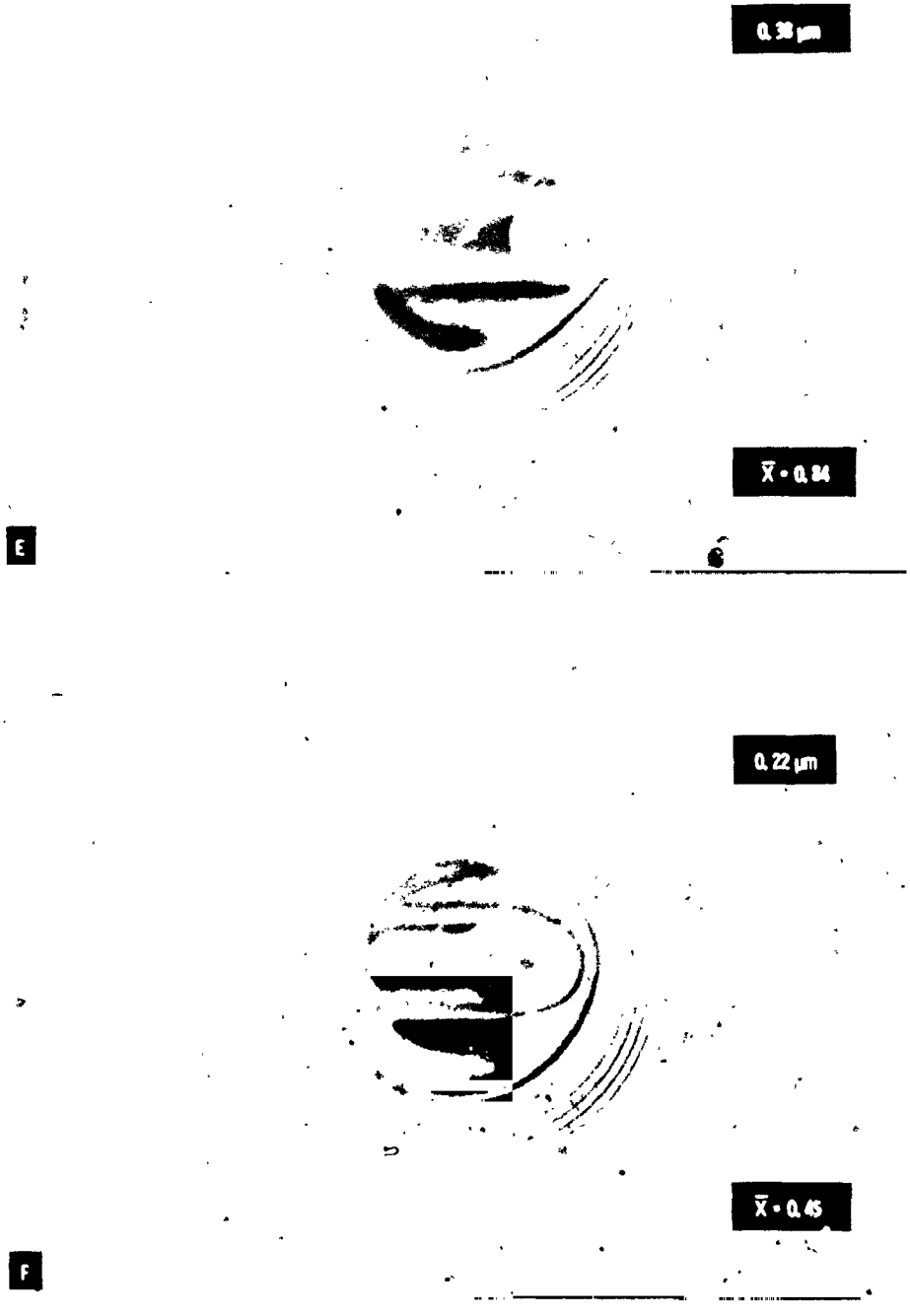

Figure 8. - Continued.

Figure 8. - Concluded.

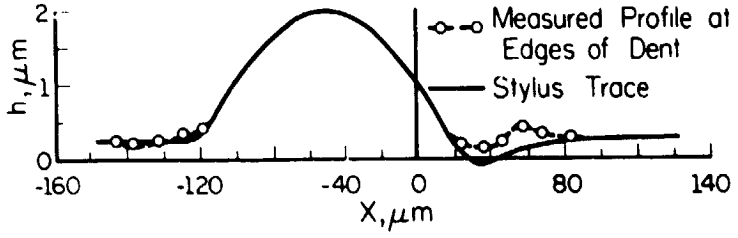

Figure 9. - Comparison of measured profile and stylus trace at edges of dent shown in figure 8(g).

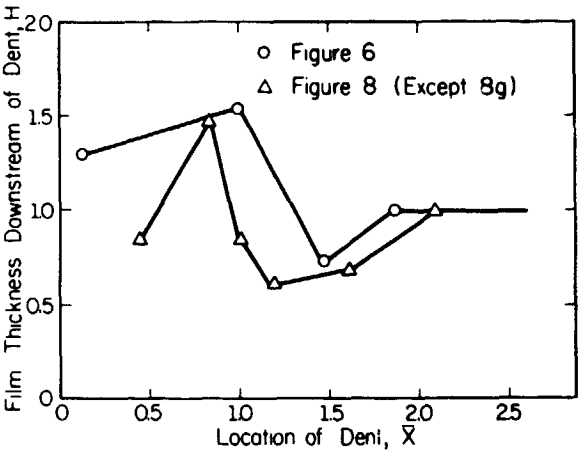

Figure 10. - Film thickness variations for dents shown in figures 6 and 8.

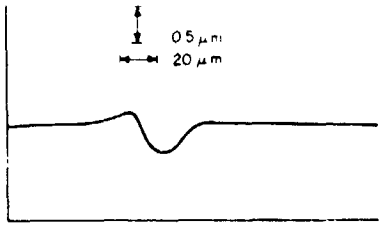

Figure 11. - Stylus trace of shallow transverse groove, Δ = 1.4, C = 0.11.

ORIGINAL PAGE
BLACK AND WHITE PHOTOGRAPH

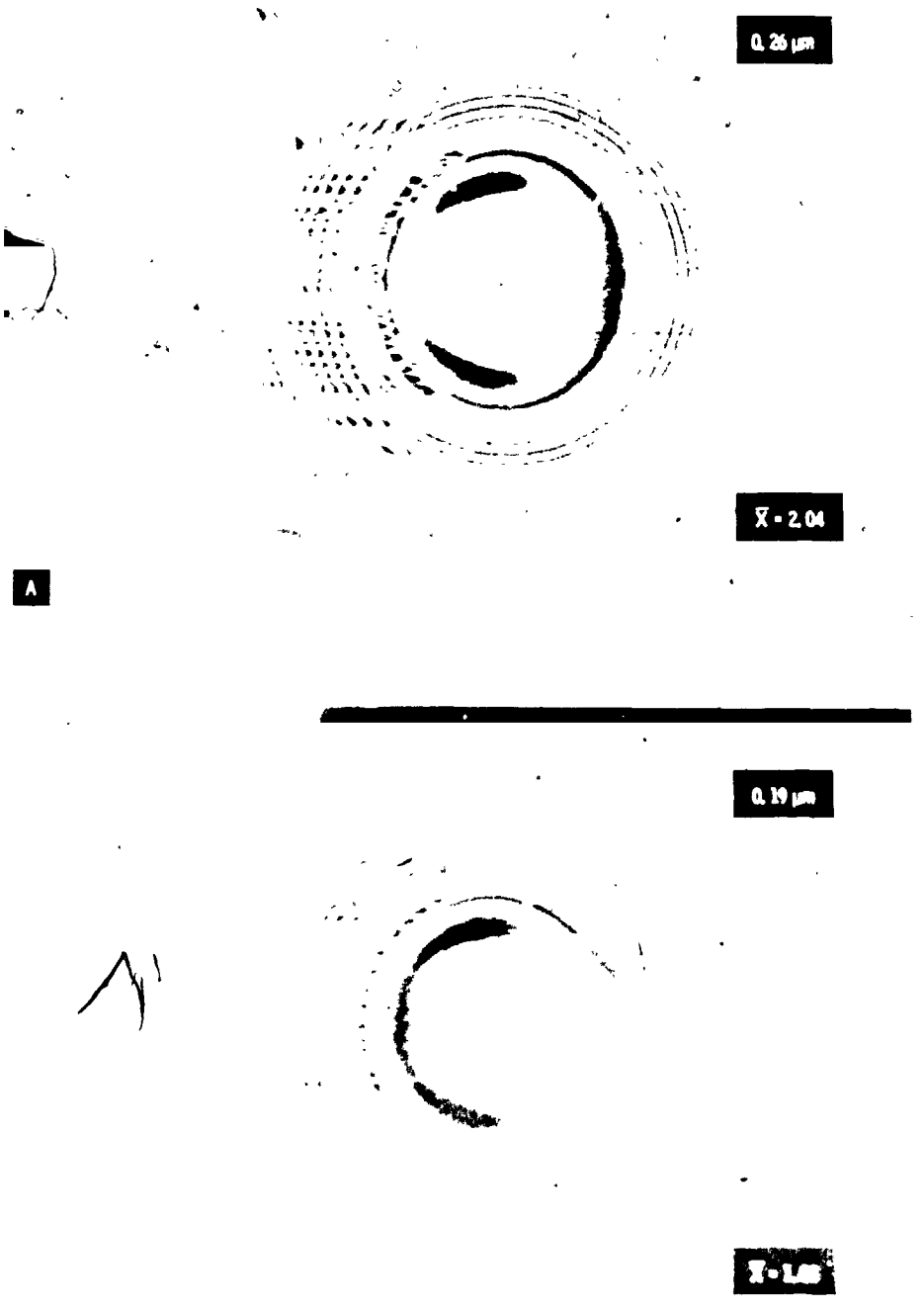

Figure 12. - Groove progressively positioned closer to inlet and in contact. Disk velocity = 0.12 m/s, P_{max} = 1.13×10^9 N/m^2, T = 24.4° C.

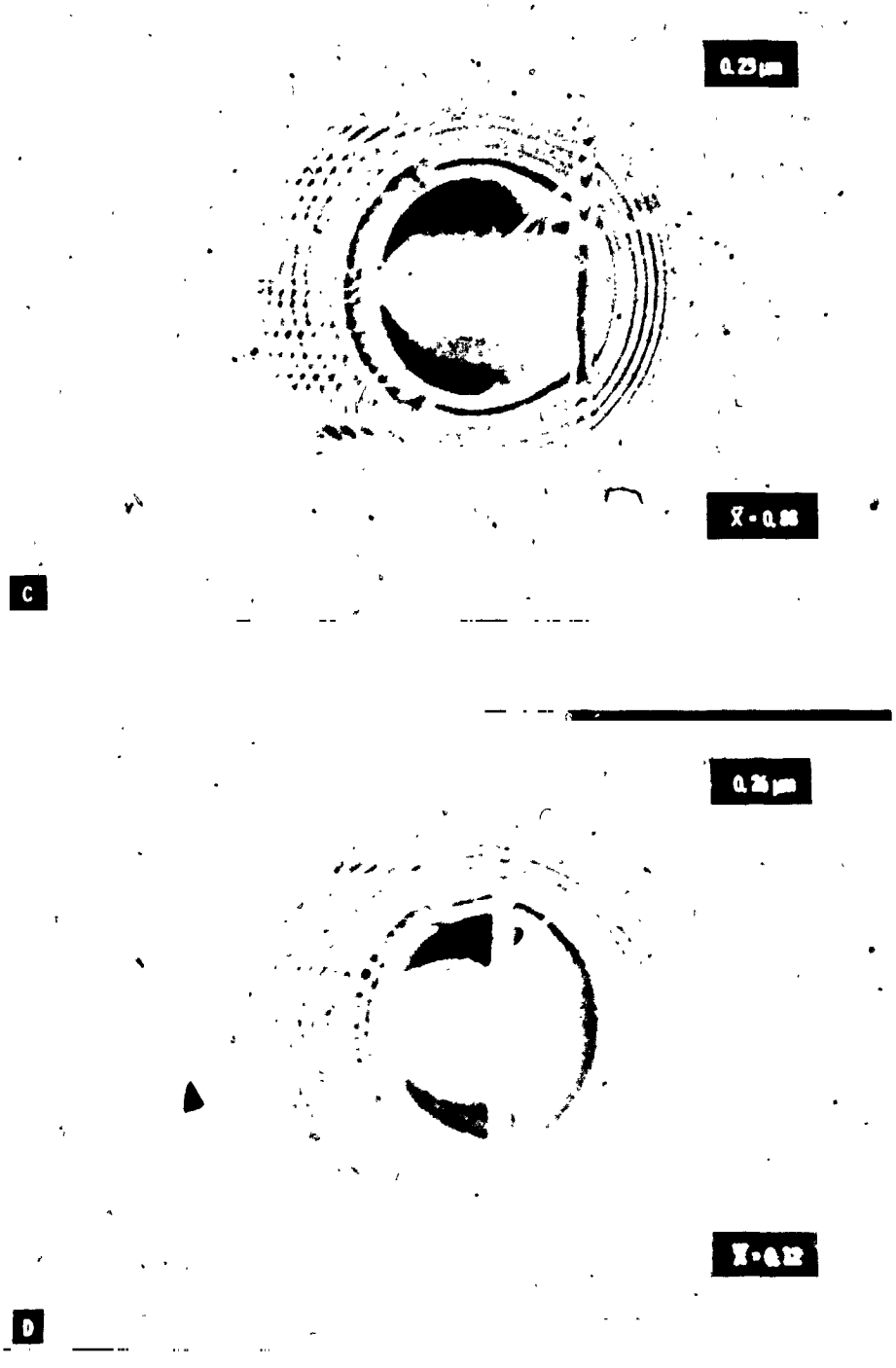

Figure 12. - Concluded.

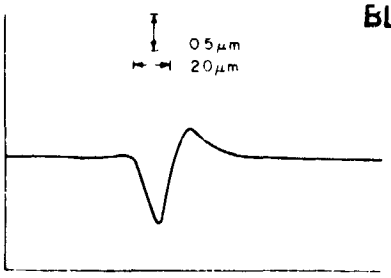

Figure 13. - Stylus trace of deep transverse groove, $\Delta = 3.4$, $C = 0.08$.

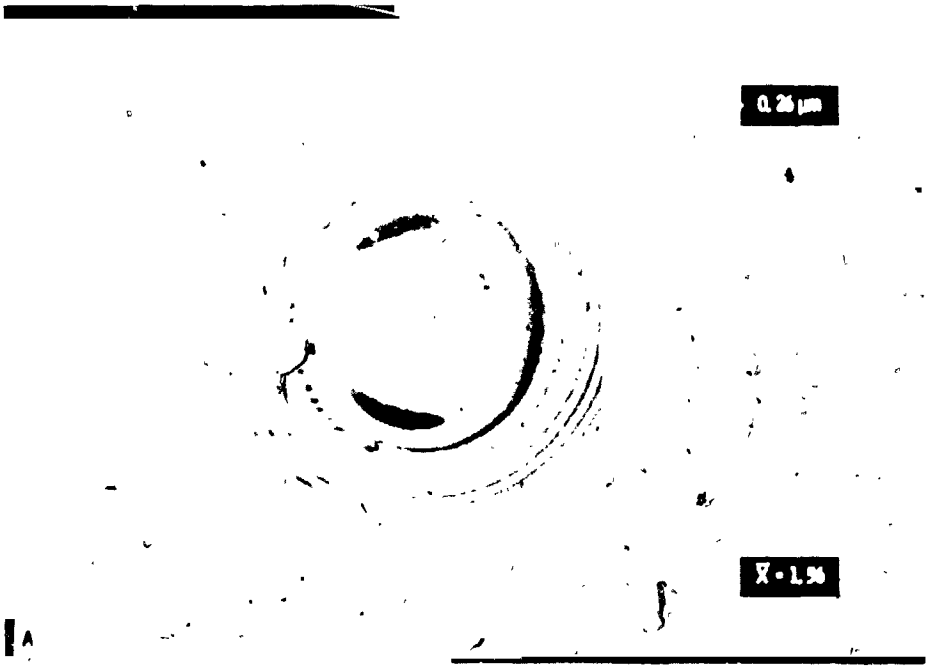

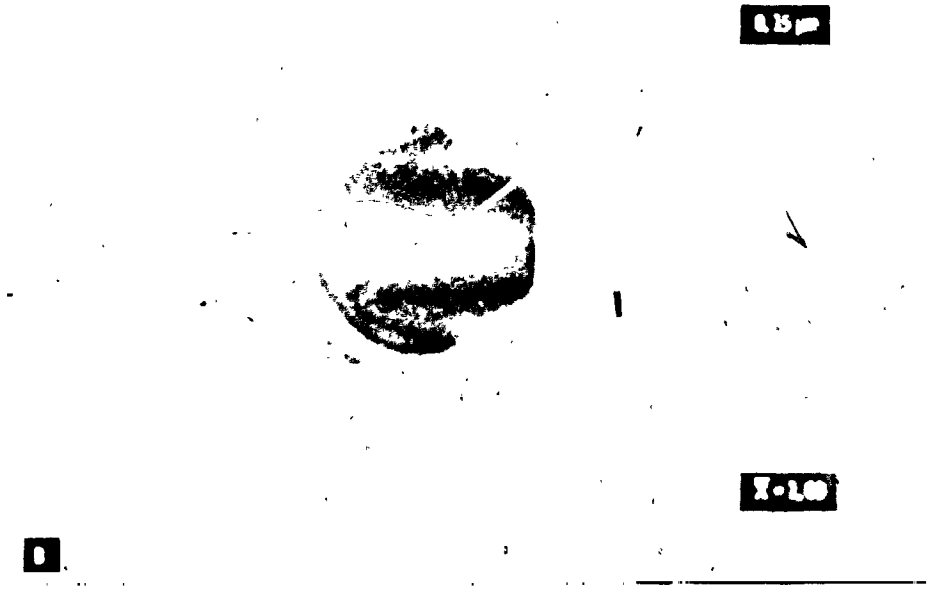

Figure 14. - Groove progressively positioned closer to inlet and in contact. Disk velocity = 0.12 m/s, $P_{max} = 1.13 \times 10^9$ N/m^2, T = 24.4° C.

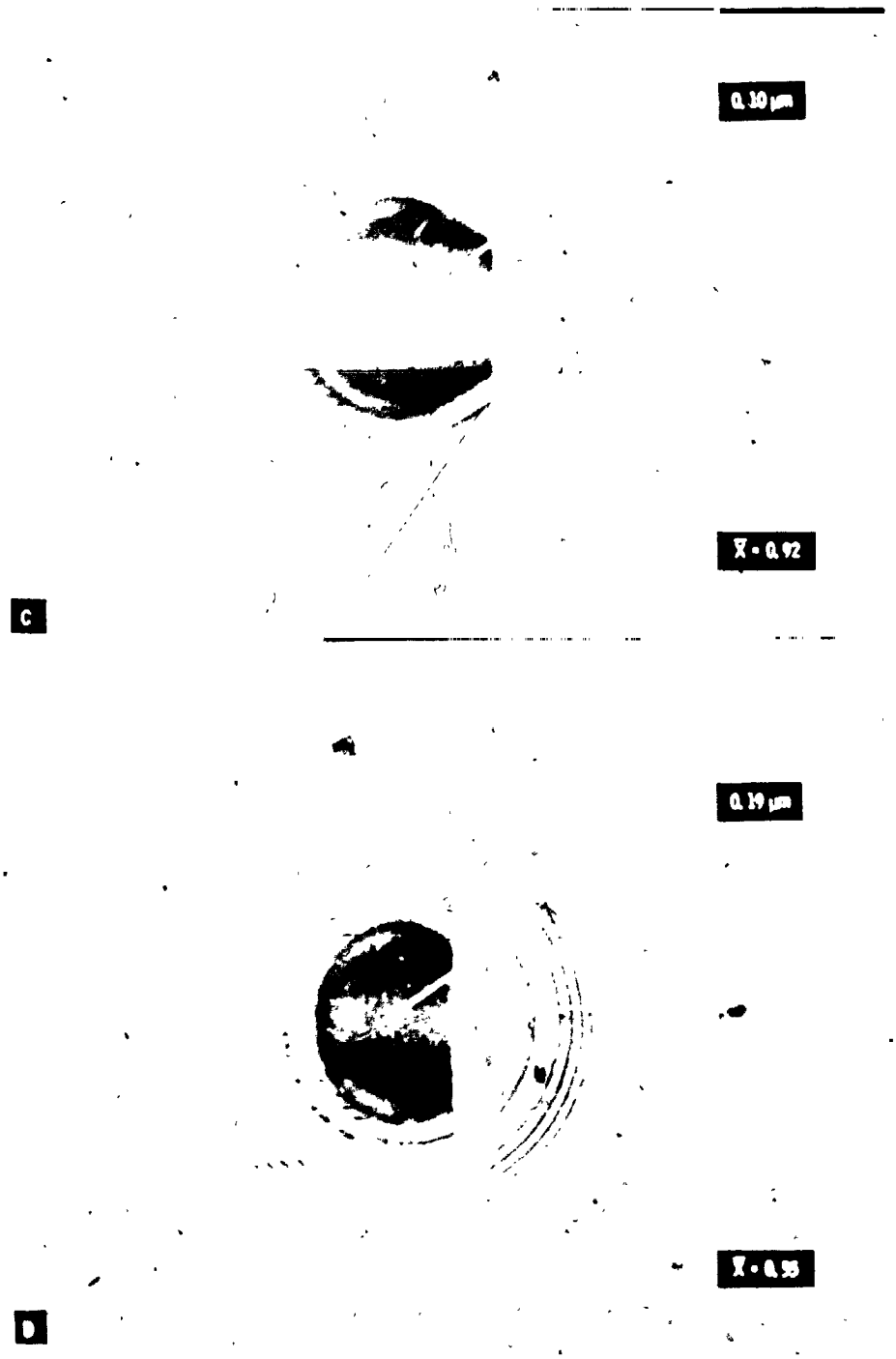

Figure 14. - Continued.

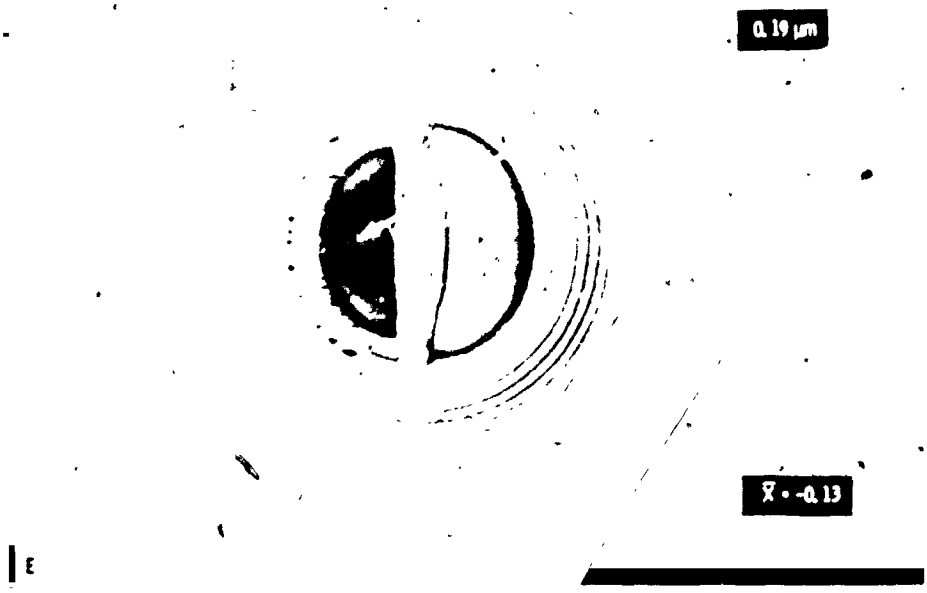

Figure 14. - Concluded.

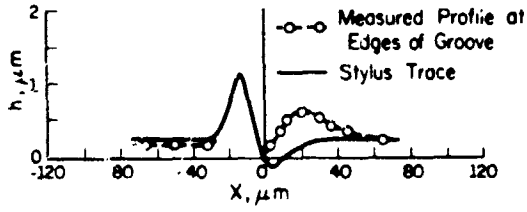

Figure 15. - Comparison of measured profile and stylus trace at edges of groove shown in figure 14(e).

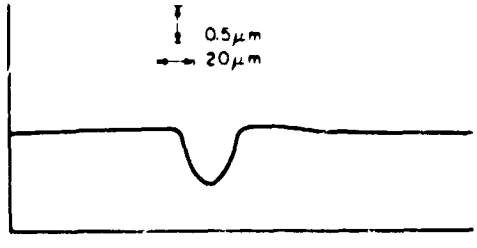

Figure 16. - Stylus trace of a longitudinal groove, Δ = 2.7, C = 0.12.

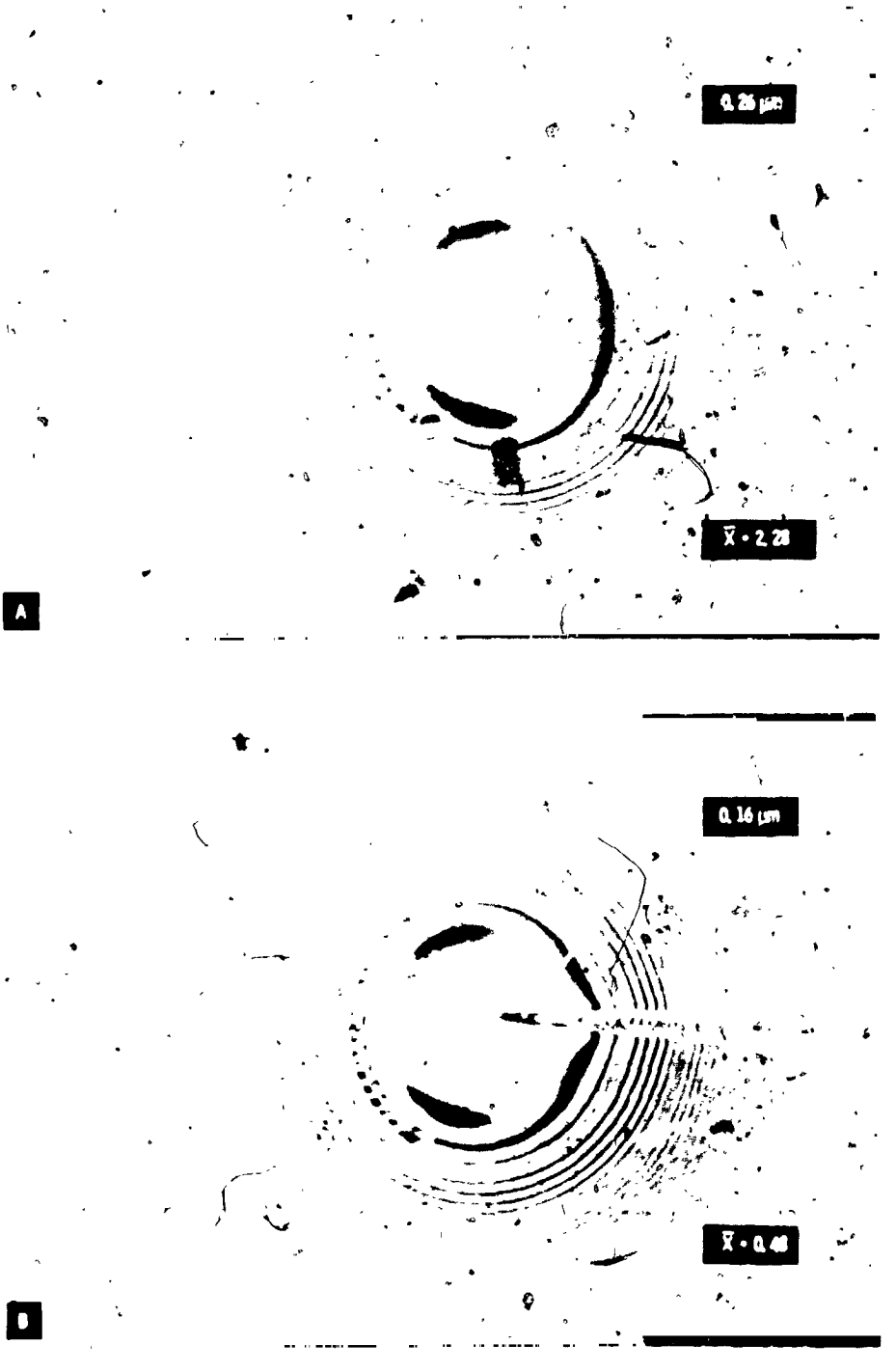

Figure 17. - Groove progressively positioned closer to inlet and in contact. Disk velocity = 0.12 m/s, P_{max} = 1.13x10^{7} N/m^{2}, T = 24.4° C.

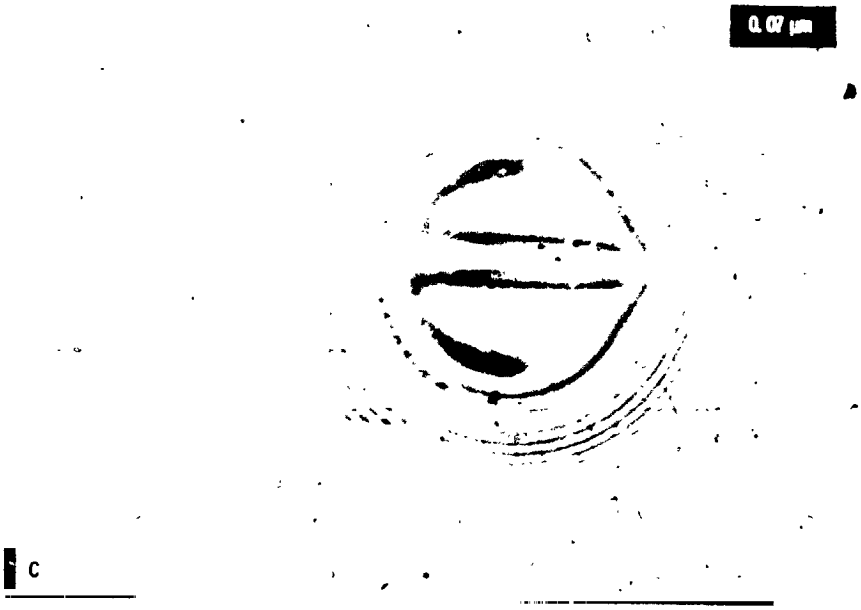

Figure 17. - Concluded.

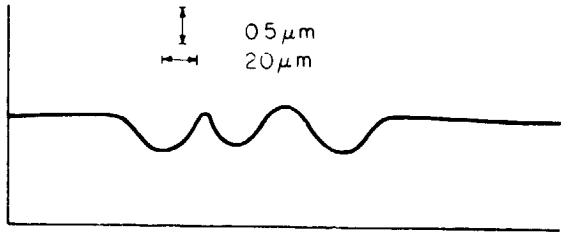

Figure 18. - Stylus trace of three transverse grooves, Δ = 2.8, C = 0.15.

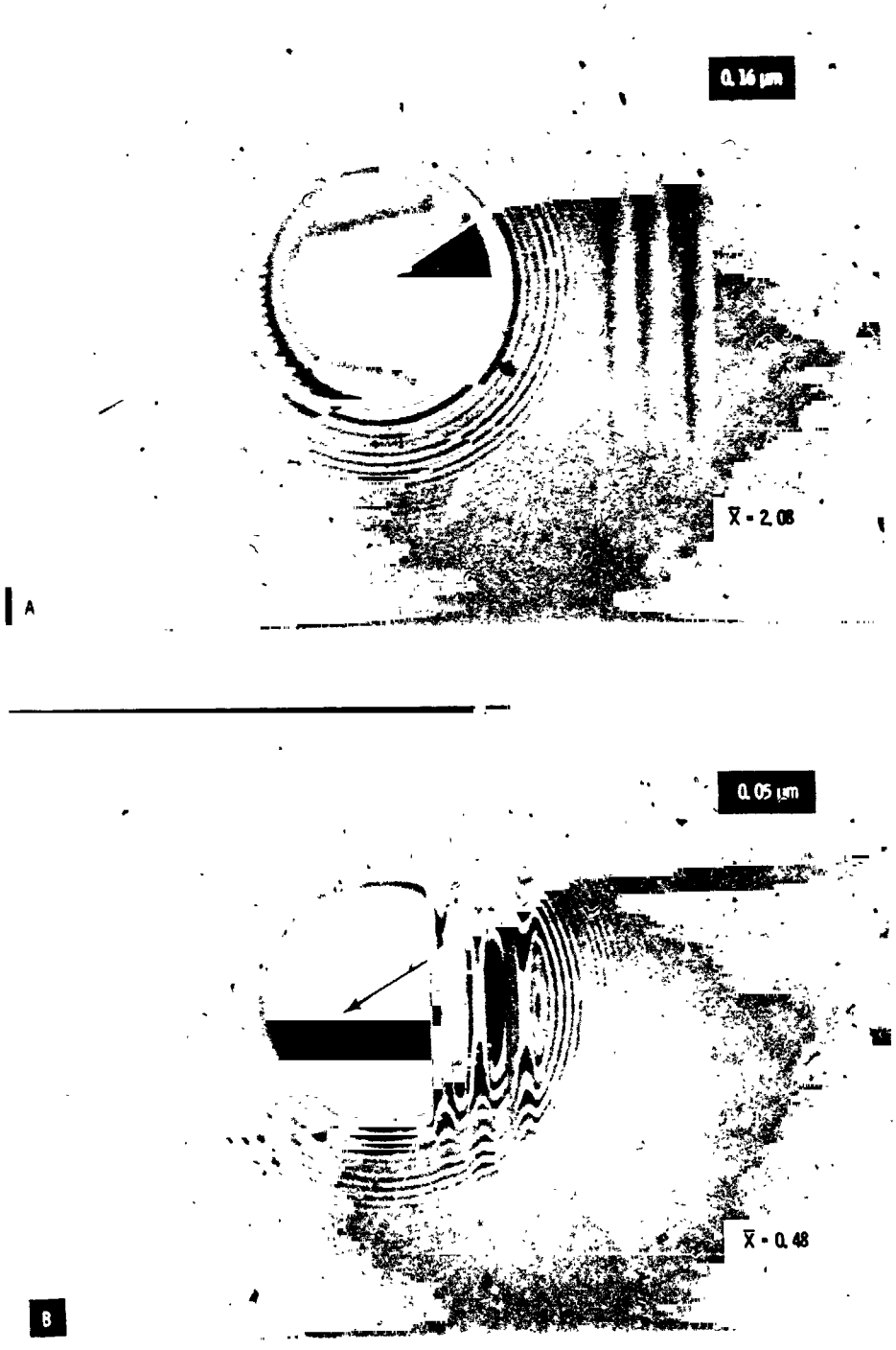

Figure 19. - Grooves progressively positioned closer to inlet and in contact. Disk velocity = 0.05 m/s, P_{max} = 1.13x10^{9} N/m^{2}, T = 28.3^{0} C.

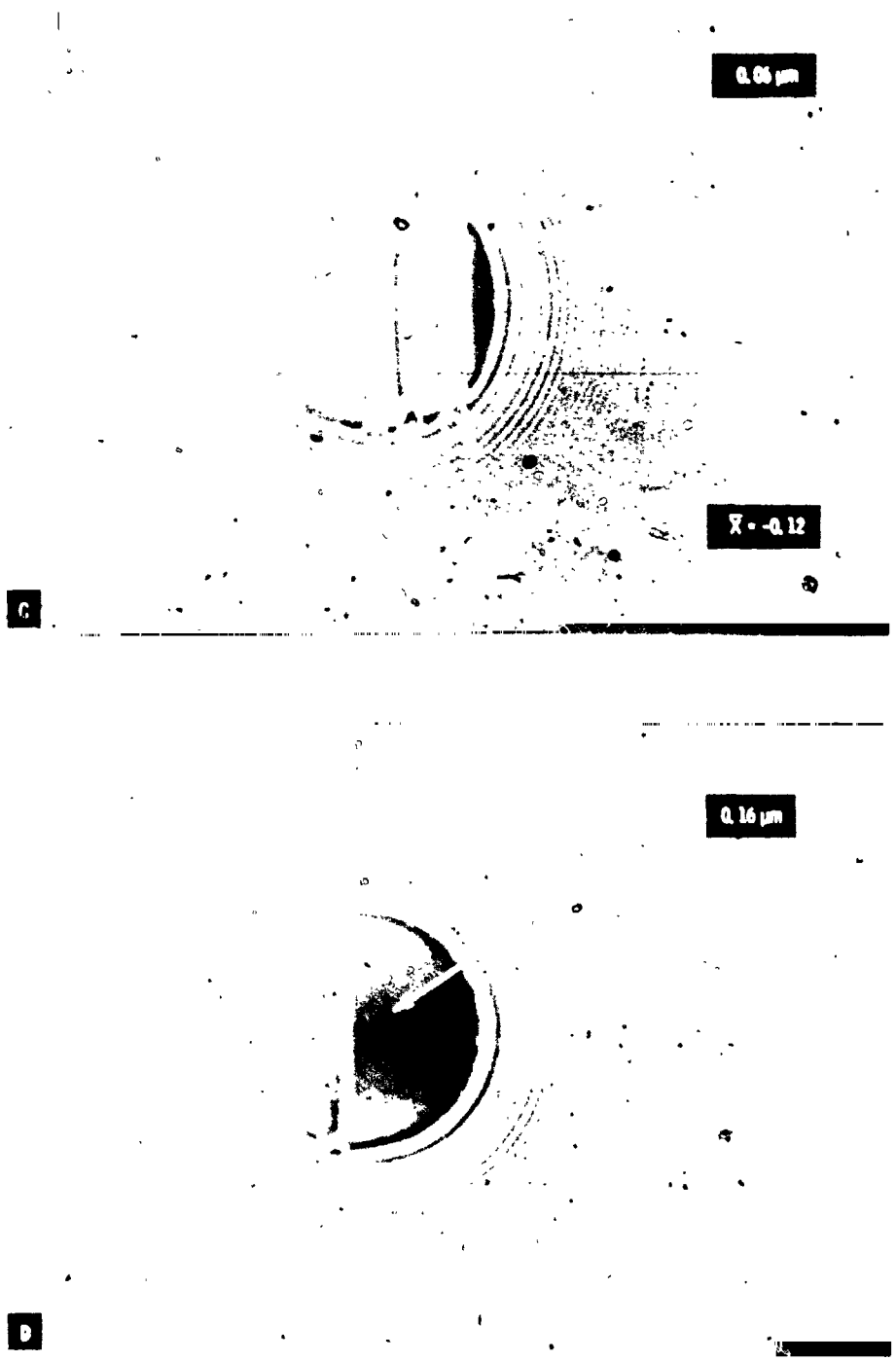

Figure 19. - Concluded.